Design and Seakeeping Performance of a Shallow-sea Surface Litter Collection Device

Design and Seakeeping Performance of a Shallow-sea Surface Litter Collection Device

Xiangyu Zhang[1], Sheng Zhang[1], Yu Lei[2], Xiangyuan Zheng[1*]

[1] Institute for Ocean Engineering, Tsinghua Shenzhen International Graduate School, 518055 Shenzhen, China

[2] China Huaneng Clean Energy Research Institute, 102209 Beijing, China

*xiangyu-20@mails.tsinghua.edu.cn; s-zhang20@mails.tsinghua.edu.cn; lei_y16@163.com; zheng.xiangyuan@sz.tsinghua.edu.cn

Abstract. In recent years, the pollution of ecological waters, especially the litter floating on the ocean surface, has emerged as a pressing economic, political, and environmental concern of the international society. The development of a widely applicable, safe, reliable and cost-saving marine surface litter collection device has drawn considerable attention. In this paper, an innovative shallow-sea floating surface litter collection device (later referred to as SFSLCD) is proposed first, including its concept design, dimensions and key parameters, working scheme, and mooring system. Second, the hydrostatic and hydrodynamic characteristics of SFSLCD are derived through numerical modeling. Last, the safety of SFSLCD in normal and rough sea states is validated in terms of its good seakeeping performance using the coastal condition of Dapeng Bay, Shenzhen, China. It is proven that this litter collection device equipped with photovoltaic panels to supply power can operate in waters of depth between 5 and 15 m in seas, rivers and lakes.

1. Introduction

Marine litter is the persistent, man-made or processed solid waste in the marine and coastal environment [1]. Since the 1850s, the scale of marine litter has been keeping rising, and the hazards of marine litter have spread to almost the whole world [2], especially, floating plastic litter is one of the most harmful forms of marine litter. In Shandong province, China, for example, the densities of large and very large pieces of floating litter in the coastal waters of Qingdao and Rizhao are 104 and 12 pieces/km^2 respectively, while the densities of medium and small pieces of floating litter are 7,727 and 6, 222 pieces/km^2 respectively [3] (the classification of litter size is based on the Technical Regulations for Monitoring and Evaluation of Marine Litter [4]). According to Jambeck's simulation [5], about 4.8–12.7 million tons of plastic litter enter the ocean every year. As plastic is hard to degrade, it is predicted that by 2050 the weight of plastic in the marine environment will surprisingly exceed the weight of fish [5]. Therefore, collecting floating litter is a very urgent task for human beings.

There are many existing successful methods to collect surface litter in inland rivers and lakes, but none of them can be readily applied in the marine environment with sea waves and current wind. The drawbacks of manual salvage collection include low efficiency and potential danger [6]. Interception cables [7] are a flexible floating boom formed by connecting floats and flexible pipes, which is only applicable to water areas with fixed or enclosed water flow direction. The "sea bin" [8] uses a water pump to create a water level difference, allowing floating litter to flow into the "bin". However, at present it can only be fixed on the shore with a small diameter and low collection volume and requires

an additional power supply. Various forms of garbage-cleaning ships have been in use, yet their construction and operation costs are high. Small unmanned collection boats have also emerged, but they cannot be adapted to the rough marine environment. Several studies on optimizing floating litter collection schemes in rivers and lakes have been carried out. For example, Wen [9] and Chen et al. [10] optimized the paddle wheel structure of cleaning ships. Thomson et al. [11] designed a multi-row rake spike collection device to increase the collection speed. Caliceti et al. [12] designed a collection device by improving the pressing method to achieve rapid dewatering of marsh moss. However, so far, the research on marine litter cleaning methods and/or devices in the world is in its early stage. An effective, economical and reliable device must be developed.

Thereof, a brand new shallow-sea floating surface litter collection device (SFSLCD) is proposed to meet the present demand. The following section presents the concept of this device that has been patented in China. The main difference between SFSLCD and the aforementioned shore or harbor fixed sea bin [8] is that SFSLCD keeps floating during service. Sections 3 and 4 respectively address the hydrostatic and hydrodynamic characteristics of this floater. Section 5 is devoted to the dynamic simulation of SFSLCD's motions in the coastal area of Dapeng Bay, Shenzhen, China. The simulation results are illustrated to affirm the good seakeeping performance in various sea conditions. Finally, concluding remarks and the future outlook are given.

2. Concept and Design of SFSLCD

2.1 Concept

The concept of SFSLCD is shown in Fig. 1. It includes four collection boxes, a photovoltaic module, pontoons, columns and braces. The photovoltaic module includes photovoltaic panels and a truss support structure sitting on columns. The photovoltaic panels are also designed to facilitate rainwater slippage. Pontoons are hollow reinforced concrete structures. They help to lower the whole center of gravity (CG) of SFSLCD. Also, pontoons are in multi-crosses such that sufficient bending and torsional strengths are guaranteed. Five columns are vertically on the pontoons. They are made of thin-walled stainless steel. Braces are used to reinforce the connections of columns with the truss support of photovoltaic panels and with pontoons.

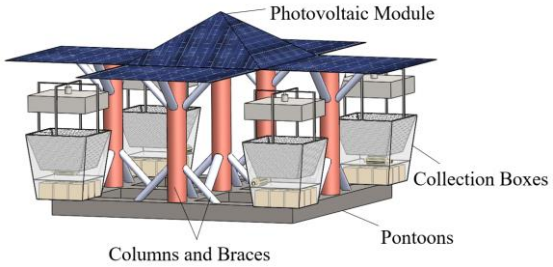

Fig.. 1. Illustration of the SFSLCD concept.

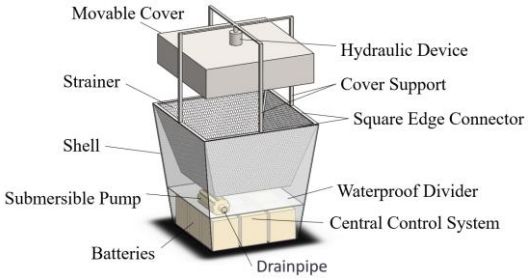

Fig.. 2. Illustration of a collection box.

The collection box shown in Fig.. 2 comprises a detachable part and a fixed part. The detachable part includes a hydraulic device, a movable cover, a cover support, a square-edge connector and a strainer.

The fixed part consists of an outer shell, a submersible pump, a waterproof divider, a central control system and batteries all contained inside the shell. A drainpipe is connected and controlled by the submersible pump. The detachable part can be lifted as a whole, while the fixed part is welded to the pontoons.

2.2 Dimensions and Key Parameters

Iterative calculations are carried out to determine a reasonable geometry of SFSLCD to achieve a balance between safety, functionality and economy. The safety considerations include structural strength, stability, and seakeeping motions. The outcome of the iterative calculation is given in Table 1. In terms of the dimensions and working modules of SFSLCD, the estimated cost of a single device is about USD 50, 000. If SFSLCD is deployed to the coastal waters of Qingdao and Rizhao mentioned in Section 1, it can ideally collect 7, 500 pieces of floating litter per day [3].

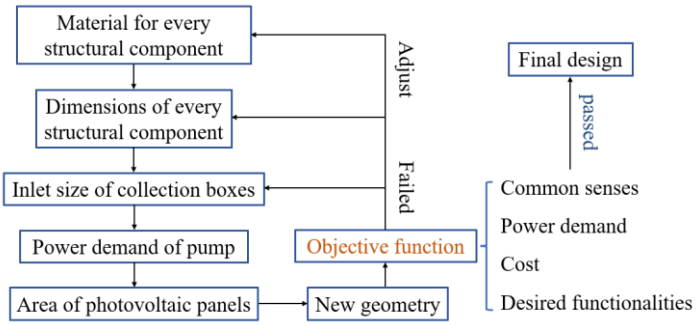

Fig.. 3. The iterative process to determine dimensions and key parameters for SFSLCD.

Table 1. Parameters of each component in a single collection box.

Component	Dimensions / Parameters	Mass (kg)
Shell	Aluminum alloy, wall thickness 0.01 m, height 2 m, top side length 2 m, bottom side length 1.5 m	565.6
Batteries	7 pcs, 69 kg, power storage 3.4 kWh	483.0
Submersible pump	Power 1.5 kW, flow rate 200 m^3/h, delivery head 1.5 m	50.0
Central control system	/	50.0
Strainer	/	150.0
Movable cover and support	Aluminum alloy, wall thickness 0.005 m	349.3
Contained water and litter	/	2, 130.8
Overall	Displacement volume 6.247 m^3	3, 778.7

Table 2. Components of SFSLCD.

Component	Dimensions / Parameters	Mass (kg)	Displacement volume (m^3)
Collection boxes	/	15, 114.7	24.988
Photovoltaic panels	Weight 56 kg/m^2, total area 90 m^2	5, 040.0	/
Central column	Stainless steel, height 5 m, diameter 0.6 m, wall thickness 0.003 m	220.8	0.571
Secondary columns	Height 4 m, others same as central column	706.7	2.285
Braces	Stainless steel, length 1.4 m, diameter 0.3 m, wall thickness 0.002 m	665.1	1.613
Pontoons	Reinforced concrete, length 8 m, width 0.8 m, height 0.5 m, bottom wall thickness 0.12 m, others 0.09 m	25, 173.7	16.320
Overall	/	46, 921.0	45.777

2.3 Working Scheme

When SFSLCD starts to work, the central control system orders the hydraulic devices to lift the movable covers up to 0.7 m above the water surface. Since the water surface is higher than the square edge connectors by 2 cm, the seawater will pour into the collection boxes with floating litter. The litter of a certain size and above is then retained on the strainers, while the inflow water goes through the strainers down to the cabins of submersible pumps. The water in cabins is then discharged off the outer shells by the submersible pumps through the drainpipes. In every collection box, there is a sensor installed onto the upper surface of the waterproof divider for monitoring the seawater pressure. Assisted by this pressure sensor, the central control system can control the drainage rate of the submersible pump. In a harsh sea state, the water inflow rate is greater than the maximum drainage rate. Thus, to ensure a stable draft of SFSLCD, the movable covers drop automatically to the square edge connectors and then seal the shells.

When the litter collection is accomplished, the central control system transmits a signal to a land-based computer server. Then a service boat is equipped with a crane departs for SFSLCD. The crane grabs the cover supports and then lifts the detachable parts onto the boat for litter cleaning.

2.4 Mooring System

The single anchor leg mooring is selected. A steel cable connects the buoy with the device (Fig. 4), allowing the device to move about the mooring center when driven by waves. The buoy can cushion the impact force from SFSLCD. A mooring chain connects the buoy and subsea pile foundation.

In the present study, the assumed water depth is 10 m. The mooring system uses a R4 non-gear mooring chain, 8.5 m long and 0.05 m in diameter. The buoy's height is 2 m and its diameter is 1 m. The steel cable is a 6 x19 strand with a length of 5 m and a diameter of 0.04 m.

3. Hydrostatic Characteristics of SFSLCD

To facilitate the discussion, the coordinate system O-X-Y-Z is defined as shown in Fig. 4. The origin of the coordinate system, O, is located at the intersection of the buoy with the calm surface. The X-axis points to the 0° incident direction of the waves. The Z-axis is vertically upward from the original point. The Y-axis is so determined by ac the right-hand rule. The 6-degree-of-freedom motion displacements of SFSLCD are defined as follows: Surging for motion along X-axis, Swaying for motion along Y-axis, Heaving for motion along Z-axis, Rolling for rotation around X-axis, Pitching for rotation around Y-axis, and Yawing for rotation around Z-axis.

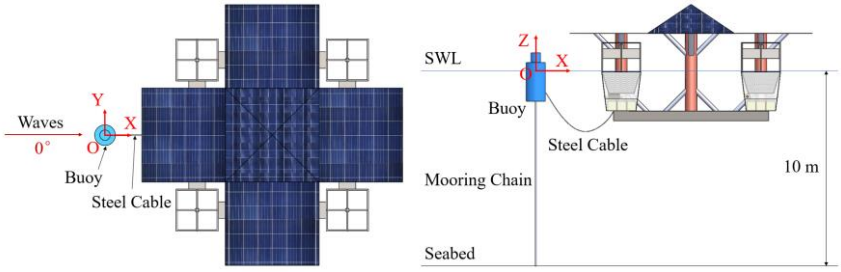

Fig. 4. Definition of the coordinate system.

Table 3. Overall properties of SFSLCD in static equilibrium.

Properties	Parameter	Properties	Parameter
Mass	46, 921.00 kg	Displacement volume	45.777 m^3
Z_{CG}	-1.392 m	Z_{CB}	-1.424 m
Roll moment of inertia	516, 127.26 kg·m^2	Draft depth	2.520 m
Pitch moment of inertia	516, 127.26 kg·m^2		
Yaw moment of inertia	838, 589.34 kg·m^2		

Table 3 lists the overall properties of SFSLCD in static equilibrium, where the positions of CG and the center of buoyancy (CB) are defined in the O-X-Y-Z coordinate system, and the origin of the calculation of the moments of inertia is located at CG. The CG of SFSLCD is slightly higher than that of CB. The static stability curve is calculated by using the software MultiSurf [13], and the result is presented in Fig. 5. The righting moment increases continuously when the inclination range is lower than 38°, implying excellent stability of this device during towing.

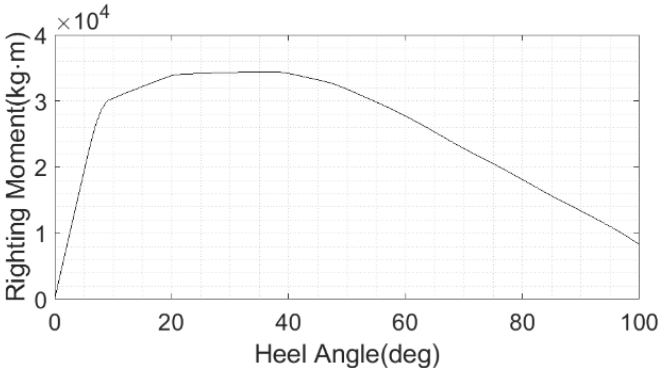

Fig. 5. Static stability curve of SFSLCD.

4. Hydrodynamic Modeling of SFSLCD

4.1 Hydrodynamic Frequency Domain Response Analysis

In this section, the hydrodynamic frequency domain analysis of SFSLCD is carried out first to study the seakeeping performance. The results of the frequency domain analysis are usually normalized to the incident wave amplitude and the transfer function is used to represent the response amplitude of the structure under waves of different frequencies and a unit wave amplitude. For first-order hydrodynamic problems, the transfer function is often referred to as the response amplitude operator (RAO) [14].

The first-order hydrodynamic analysis is carried out in WAMIT [15]. To improve the computational accuracy, a high-order geometric panel model is used (Fig. 6). Since the foundation of SFSLCD is symmetric, only 1/4 of the model is required in geometric modeling. Considering that the brace diameters are at least 1 order of magnitude smaller than the commonly encountered wavelength, braces are ignored in solving the potential flow problem.

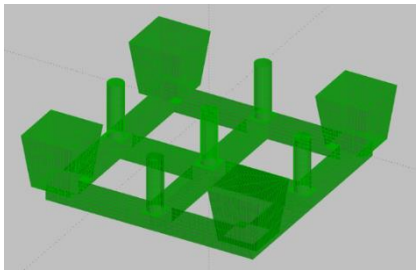

Fig. 6. High-order panel model for SFSLCD.

After sensitivity analysis, the grid panel size of 0.2 m is adopted. The RAO results of SFSLCD in the free-floating state without considering the viscous damping, under 0° incident waves are shown in Fig. 7 (wave period range of 1.5 to 15 s and interval of 0.1 s). It should be noted that the model here only includes radiation damping, so the amplitudes of the motions near the natural periods are very large. It can be observed that SFSLCD has a natural heave period of 4.3 s and a natural pitch period of 3.7 s, both close to short wave periods in near-shore areas.

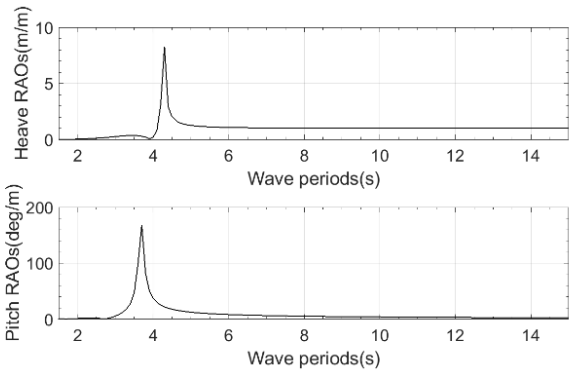

Fig. 7. Heave and pitch RAOs (free-floating state, potential flow only).

4.2 More Complete Time-domain Coupled Numerical Model

To account for viscous drag damping, a hybrid model combining potential flow forces and Morison drag forces is developed. In OrcaFlex [16], SFSLCD is assumed to be a 6-degree-of-freedom rigid body, and a user-defined "vessel" is used to simulate it. The first-order wave forces RAO with added mass coefficients, radiation damping coefficients and hydrostatic coefficients of "vessel" are calculated in WAMIT (as shown in Sec. 4.1), while Morison drag forces are added into this "vessel" model for modeling the hydrodynamic loads on slender members like braces. In OrcaFlex, all Morison element models are simplified as cylinders whose drag coefficients C_d are selected according to DNV [17] and [18].

Table 4. Drag force coefficient C_d.

Component	Longitudinal	Transverse	Vertical
Column	1.00	1.00	0.82
Brace	1.00	1.00	0.82
Pontoon	1.60	2.50	0.82
Collection box	1.05	1.05	1.05

In OrcaFlex, the mooring chain and steel cable are simulated by "line" units, and the buoy is simulated by a "6D buoy" unit. The bending stiffness and torsional stiffness of the mooring chain and steel cable are zero, so only its axial stiffness is considered in simulations. The Morison equation [19] is used to calculate the hydrodynamic force on the mooring chain. The horizontal wave force on a unit length of an upright cylinder can be written as the following Morison equation in a coupled style:

$$f = \frac{1}{2} C_d \rho D (u_x - \dot{x}) |u_x - \dot{x}| + (1 + C_a) \rho \frac{\pi D^2}{4} a_x - C_a \rho \frac{\pi D^2}{4} \ddot{x} \quad (1)$$

where u_x and a_x are the horizontal velocity and acceleration of the water quality point, respectively; ρ is the seawater density; D is the cylinder diameter; C_a is the additional mass coefficient; $\dot{x}$ and $\ddot{x}$ are the horizontal velocity and acceleration of cylinder motions respectively.

According to the specification [17], the added mass coefficient (C_a) of the chain is 1.0 and C_d is 2.4. For the steel cable, C_a is 1.0 and C_d is 1.2. For the buoy, the tangential C_a is 1.0, and the axial C_a is 0.23, the tangential C_d is 1.0, and the axial C_d is 0.82.

At this point, the numerical model of SFSLCD in the moored state, considering the drag force, is established in OrcaFlex. The hydro-elastic coupled dynamic responses of all components are calculated by the finite element method.

5. Dynamic Response of SFSLCD

5.1 Environmental Conditions and Load Cases

The potential operating area of SFSLCD is Dapeng Bay in the South China Sea with specific coordinates of E114.4° and N22.5°, which is adjacent to Shenzhen city, with an average water depth of 10 m. The

corresponding ocean hydrographic data of this area is provided by the ERA-5 dataset in the Copernicus climate database [20]. The 1-year and multi-year extremes of mean wind speed and wave height are assumed to obey the Gumbel distribution [17] to obtain H_s (significant wave height) and U_{10} (10-min mean wind speed at an altitude of 10 m) for the 1-year and multi-year events, and the conditional probability density functions of H_s and T_1 (mean wave periods) are assumed to follow the lognormal model [21]. T_p (peak wave periods) is then determined according to the relationship [17] between T_p and T_1. The stochastic waves in the target sea are assumed to follow the Pierson-Moskowitz spectrum [17], and then multiply the depth correlation function $\phi(\omega)$ to form the TMA spectrum by considering the effect of water depth, whose key spectral parameters for the three loading cases (LC) are shown in Table 5. These load cases correspond to the normal, 1-year return and 5-year return sea conditions respectively. LC3 is the most severe sea condition that SFSLCD can survive. In this study, it is assumed that the seabed is flat and horizontal.

Table 5. Load cases.

Load Case	H_s (m)	T_p (s)	Description
LC1	0.27	4.79	Normal operating condition: stochastic waves
LC2	1.42	6.17	1-year return stochastic waves
LC3	1.67	6.73	5-year return stochastic waves

5.2 Results of Dynamic Responses

For each load case, three numerical simulations of 8, 200 s are carried out, and the first 1, 000 s results of the simulation are discarded to eliminate the effect of transients, so the effective simulation time for each case is 6 hours, corresponding to the steady-state response. Table 6 gives the dynamic response statistics of SFSLCD in LC1, LC2 and LC3 (normal operating, 1-year and 5-year return stochastic waves, respectively). The effective tensions of the mooring chain and the steel cable are respectively denoted as T_{chain} and T_{cable}.

Table 6. Comparison of response statistics in LC1, LC2 and LC3.

Load Case	Variables	Surge (m)	Heave (m)	Pitch (deg)	T_{chain} (kN)	T_{cable} (kN)
LC1	Mean	2.218	-0.001	-0.009	10.234	0.111
	Maximum	2.558	0.244	4.677	11.428	0.119
	Minimum	1.842	-0.233	-4.500	8.842	0.101
	Std. deviation	0.115	0.061	1.376	0.325	0.002
LC2	Mean	5.586	0.001	0.049	10.695	1.233
	Maximum	7.982	1.306	14.989	108.736	223.415
	Minimum	4.150	-1.119	-15.091	-0.655	-0.013
	Std. deviation	0.486	0.321	4.211	2.239	6.237
LC3	Mean	6.161	0.002	0.069	11.055	1.615
	Maximum	8.937	1.406	17.556	109.509	228.214
	Minimum	4.425	-1.241	-16.689	-0.433	-0.009
	Std. deviation	0.589	0.370	4.745	2.477	6.253

The following conclusions can be drawn from this table. The displacement response of SFSLCD and the tension response of mooring cable are small in LC1 in which SFSLCD can carry out the normal litter collection work at ease. In LC2 and LC3, due to harsher wave conditions than LC1, SFSLCD experiences larger displacement (especially heave > 1.3 m) such that its litter collection ceases. T_{cable} and T_{chain} in these two load cases are large but they are still lower than the threshold value according to DNV codes [22]. In addition, there are a lot of impact tensions in the cable due to the frequent slack to tensioning (Fig. 8).

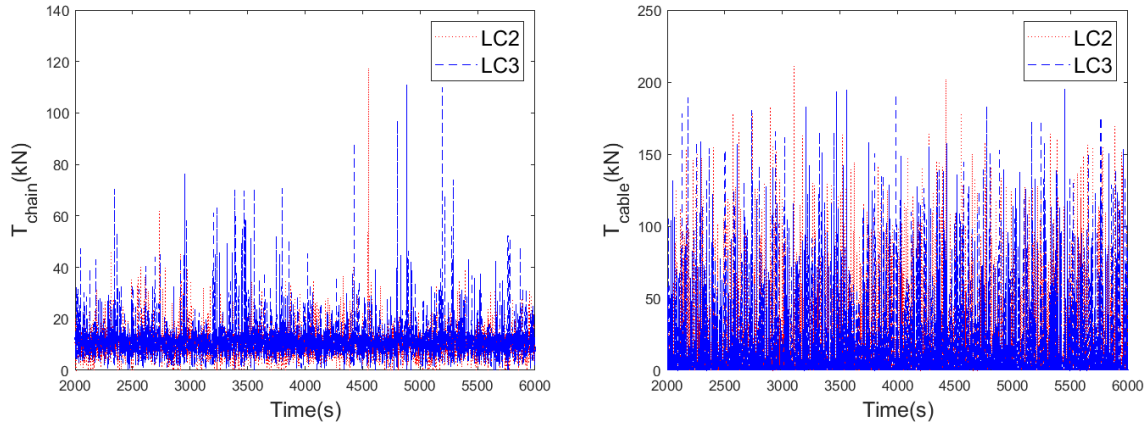

Fig. 8. The time history of T_{cable} and T_{chain} in LC2 and LC3.

LC3 is harsher than LC2 while their T_p is close. Thus, the response power spectra of LC1 and LC3 are presented. For the convenience of analysis, the natural frequencies of the heave, pitch, and surge of SFSLCD are noted as f_{heave} (0.23 Hz), f_{pitch} (0.27 Hz), and f_{surge}. The wave frequencies corresponding to T_p are denoted as f_{wave1} (0.21 Hz) and f_{wave3} (0.15 Hz). It can be observed from Fig. 9 that the power spectra of surge, heave and pitch are all peaked at their natural frequencies or the wave frequencies, and surge and pitch are coupled.

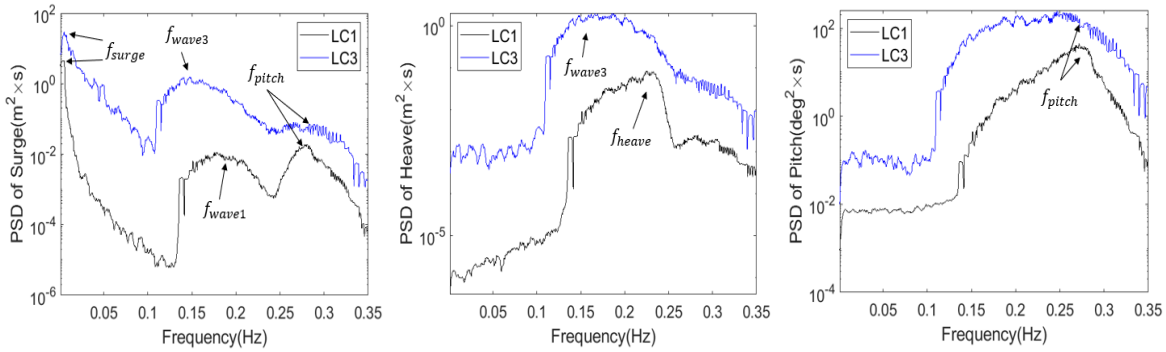

Fig. 9. The power spectra of seakeeping motions in LC1 and LC3.

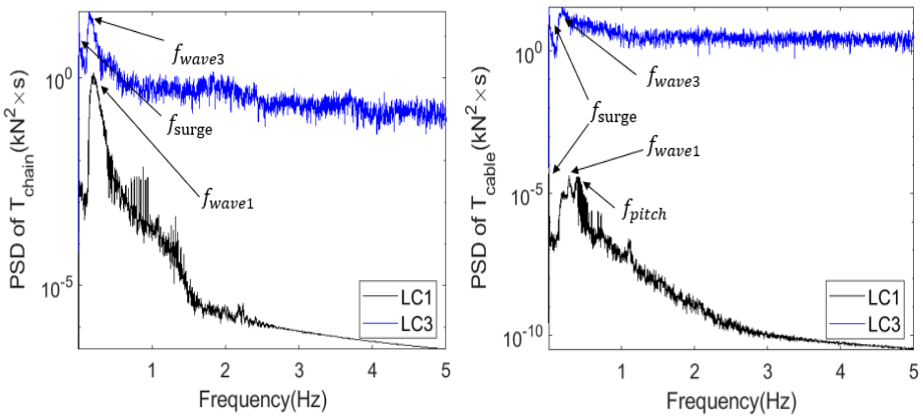

Fig. 10. The power spectra of mooring tensions in LC1 and LC3.

As illustrated in Fig. 10, the steel cable is tensioned in LC3, causing the power spectrum of T_{chain} to peak at f_{surge}, also resulting in a larger high-frequency component in the power spectrum of T_{cable} and T_{chain}.

6. Conclusions

At present, no feasible surface litter collection devices have been developed for shallow seas. The proposed concept of SFSLCD in this paper is devoted to a self-powered, safe, reliable, efficient, and cost-effective device in seas of depth between 5 and 15 m. The safety of SFSLCD in normal and rough sea states is validated in terms of its good seakeeping performance by using the coastal conditions of Dapeng Bay, Shenzhen, China. In the normal operating sea condition, the motions of SFSLCD are so small that the pumps can discharge seawater promptly to sustain the collection work.

In further research, more load cases such as the coupled wave and current condition need to be considered. Also, for commercialization, the technical feasibility of SFSLCD requires in-depth verification through experimental studies and site demo tests in coastal areas.

Acknowledgements

The financial support received from China National Science Foundation Program (52071186), the Key Promotion Program of High Quality Marine Economy Development by Guangdong Province of China (GDNRC [2022] 33) and The Major Program of Stable Sponsorship for Higher Institutions (Shenzhen Science & Technology Commission, WDZC20200819174646001) are greatly acknowledged.

References

[1] Jeftic, L., Sheavly, S., Adler, E. (2009) Marine litter: A global challenge. The United Nations Environment Programme, Nairobi. https://www.vliz.be/imisdocs/publications/ocrd/15190-8.pdf.

[2] Mao, D. (2010) A historical account of marine garbage pollution and its remedies. Journal of Yunnan Normal University (Humanities and Social Sciences), 42 (6): 56–66. DOI: 10.3969/j.issn.1000-5110.2010.06.009.

[3] Sun, W., Tang, X. C., Xu, Y. D., et al. (2016) Distribution, composition and change characteristics of marine litter in coastal waters of Shandong Province. Science, Technology and Engineering, 16 (18): 89–94. DOI: 10.3969/j.issn.1671-1815.2016.18.016.

[4] Department of Ecological Environmental Protection. (2015) Notice of the Department of Ecological Environmental Protection of the State Oceanic Administration on the Issuance of Technical Procedures for Marine Litter Monitoring and Evaluation (for Trial Implementation). Beijing. http://gc.mnr.gov.cn/201807/t20180710 _2079008.html.

[5] Jambeck, J. R., Geyer, R., Wilcox, C., et al. (2015) Plastic waste inputs from land into the ocean. Science, 347 (6223): 768–771. DOI: 10.1126/science.1260352.

[6] Wang, S. Q., Zheng, J. M., Deng J., et al. (2015) Exploration of the generation and treatment methods of river floating rubbish. Industry and Technology Forum, 14 (17): 77–78. DOI: 10.3969/j.issn.1673-5641.2015.17.042.

[7] Lin Z, M. (2016) A review of research on methods of collecting marine drifting waste in mariculture areas. Shanxi Construction, 42 (27): 182–184. DOI: 10.3969/j.issn.1009-6825.2016.27.098

[8] Parker-Jurd, F. N. F., Smith, N. S., Gibson, L., et al. (2022) Evaluating the performance of the 'Seabin'–A fixed point mechanical litter removal device for sheltered waters. Marine Pollution Bulletin, 184: 114199. https://doi.org/10.1016/j.marpolbul.2022.114199.

[9] Wen, J. (2000) Experimental study on the surface rubbish sweeper of the Pearl River. Guangdong Shipbuilding, 2000 (Z1):14–20. DOI: CNKI:SUN: GDCC.0.2000-Z1-003.

[10] Chen, J. W., Zhang, L. Z., Bao C. X. (2008) Optimization design of the open wheel of SCSGJ-2.6 type small water grass harvester. Anhui Agricultural Science, 2008 (08): 3467–3469. DOI: 10.3969/j.issn.0517-6611.2008.08.188.

[11] Thomson, Enala, T., Mwase, et al. (2002) Control of aquatic weeds through pollutant reduction and weed utilization. Physics and Chemistry of the Earth, 27 (10): 983–991. https://doi.org/10.1016/S1474-7065(02)00102-X.
[12] Caliceti, M., Argese, E., Sfriso, A., et al. (2002) Heavy metal contamination in the seaweeds of the Venice lagoon. Chemosphere, 47 (4): 443–454. https://doi.org/10.1016/S0045-6535(01)00292-2.
[13] AeroHydro, Inc. (2011) MultiSurf 8.0. Southwest Harbor. https://aerohydro.com/test/Multi-Surf_WAMIT8-master.pdf.
[14] Chakrabarti, S. K. (1987) Hydrodynamics of offshore structures. WIT Press, Billerica. DOI: 10.1016/0951-8339(88)90012-3.
[15] WAMIT, Inc. (2013) Wamit User Manual. Version 7.0. Massachusetts. http://www.wami-t.com /manualupdate/v74_manual.pdf.
[16] Orcina, Ltd. (2019) OrcaFlex User Manual. Version 11.0d. Ulverston Cumbria. https://ww-w.or-cina.com/webhelp/OrcaFlex/Redirector.htm?What%27snewinthisversion.htm #110g.
[17] DNV. (2010) DNV-RP-C205 Recommended practice: Environmental conditions and environmen-tal loads. Oslo.
[18] Nardone, P., Koll, K. (2018) Velocity field and drag force measurements of a cube and a hemi-sphere mounted on an artificial bed surface roughness. E3S Web of Conferences, 40. https://doi.org/10.1051/e3sconf/20184005022.
[19] Morison, J., Johnson, J., Schaaf, S. (1950) The force exerted by surface waves on piles. Journal of Petroleum Technology, 2 (05): 149–154. https://doi.org/10.2118/950149-G.
[20] European Centre for Medium-Range Weather Forecasts Public Dataset ERA Interim. http://apps.ecmwf.int/datasets/data/interim-full-daily/levtype=sfc/.
[21] Moan, T., Gao, Z., Ayala-Uraga, E. (2005) Uncertainty of wave-induced response of marine struc-tures due to long-term variation of extratropical wave conditions. Marine Structures, 18 (4): 359–382. https://doi.org/10.1016/j.marstruc.2005.11.001.
[22] DNV. (2015) DNVGL-OS-E301 Offshore standard: position mooring. Oslo.